

Trends in activity for the oxygen evolution reaction on transition metal (M = Fe, Co, Ni) phosphide pre-catalysts

Junyuan Xu,^a Junjie Li,^a Dehua Xiong,^a Bingsen Zhang,^b Yuefeng Liu,^b Kuang-Hsu Wu,^b Isilda Amorim,^a Wei Li,^a and Lifeng Liu^{a*}

^a *International Iberian Nanotechnology Laboratory, Av. Mestre Jose Veiga, 4715-330 Braga, Portugal*

^b *Shenyang National Laboratory for Materials Science, Institute of Metal Research, Chinese Academy of Sciences, Shenyang, Liaoning, 110016, China*

Experimental procedures

Pre-treatment of CNFs

The CNFs were purchased from Sigma-Aldrich. The as-received CNFs were pre-treated by a modified Hummers method.¹ Briefly, 1 g of CNFs was first purified by thermal annealing at 500 °C in high-purity nitrogen (N₂, 99.999 %) and then washed with 40 mL of diluted hydrochloric acid (10 wt %) to remove metal residues and amorphous carbon. The purified CNFs were repeatedly cleaned with deionized (DI) water, and were subsequently collected and dried at 80 °C in a vacuum oven for 12 h. 0.5 g of purified CNF powders was mixed with 25 mL of concentrated sulfuric acid (98 %) in a 250 mL round flask, and the solution was rigorously stirred at 25 °C for 12 h. Next, the round flask was heated to 40 °C in an oil bath, and 0.1 g of NaNO₃ and 1 g of KMnO₄ were slowly added in sequence into the flask. After stirring at 40 °C for 30 min, 3 mL of DI water was added, followed by another 3 mL after 5 min. 40 mL of DI water was slowly added in 5 min later and the temperature was maintained at 40 °C for 15 min. After the temperature decreased to 25 °C, 140 mL of DI water was poured into the solution, followed by addition of 10 mL of 30 % H₂O₂ to stop the reaction after 10 min. The as-treated CNFs were collected and washed with copious DI water until pH ≥ 5. The CNFs were then dried at 50 °C in vacuum oven for 24 h.

Synthesis of TMP pre-catalysts

The TMP pre-catalysts were synthesized by solution-based chemical reduction of corresponding metal cations in the presence of sodium borohydride (NaBH₄) and CNFs in ethylene glycol (EG) solution.² Taking FeCoNiP as an example. 0.24 g of acid-treated CNFs was firstly suspended in 30 mL of EG, and the solution was sonicated at 25 °C for 1 h. Subsequently, the EG solutions of FeCl₂·4H₂O (6.0 mL, 0.05 M Fe²⁺), CoCl₂·6H₂O (6.0 mL,

0.05 M Co^{2+}) and $\text{NiCl}_2 \cdot 6\text{H}_2\text{O}$ (6.0 mL, 0.05 M Ni^{2+}) were added, and the mixture was held at 25 °C under magnetic stirring for 3 h. Next, the solution temperature was increased to 60 °C and NaBH_4 solution (30 mL, 10 mg mL^{-1}) was slowly added under rigorous stirring. After reaction for 0.5 h, the mixture was cooled down to 25 °C, centrifuged, and rinsed several times with DI water. The as-obtained powders were dried in a vacuum oven at 80 °C for 24 h. The phosphorization was performed at 300 °C using NaH_2PO_2 as the source of phosphorus.³ Typically, 0.1 g of CNF powders coated with FeCoNi NPs was loaded in a ceramic boat, with 0.5 g of NaH_2PO_2 placed 2 cm away from the CNFs at the upstream side. Subsequently, the boat was put into a tube furnace, wherein high-purity N_2 (99.999%) was purged at a flow rate of 800 SCCM for 1 h to remove air. Afterwards, the furnace was ramped to 300 °C at a rate of 5 °C min^{-1} , held at this temperature for 2 h, and then cooled down naturally to room temperature. A constant N_2 flow was maintained in the whole process. FeP, NiP, CoP, FeNiP, FeCoP and CoNiP pre-catalysts were prepared according to the same procedure described above using the corresponding precursor metal salt(s). Supportless FeCoNiP NPs were also prepared to elucidate the impact of CNF supports on the OER activity. In this case, all synthetic conditions were kept the same except that no CNF powders were added in the solution-based chemical reduction step.

Materials characterization

Powder XRD examinations were conducted on a X'Pert PRO diffractometer (PANalytical) working at 45 kV and 40 mA with $\text{Cu } K_\alpha$ radiation ($\lambda = 1.541874 \text{ \AA}$) and a PIXcel detector. Data were collected with the Bragg-Brentano configuration in the 2θ range of 20 – 80° at a scan speed of 0.01° s^{-1} . XPS characterization was performed on an ESCALAB 250 instrument with $\text{Al } K_\alpha$ X-rays (1489.6 eV). The real metal loading on CNF was determined by ICP-MS (Agilent 7700X). Specifically, 20 mg of pre-catalysts were dispersed in 12 g of concentrated nitric acid in an autoclave, which was then kept in an electric oven at 180 °C for 12 h to completely digest carbon. Subsequently, the acid solution was diluted in a 50 mL volumetric flask. The analyses for each TMP pre-catalyst were done at least three times using *ca.* 10 mL solutions each time to obtain an average composition value. TEM, HRTEM, and STEM elemental mapping investigations were carried out on a probe-corrected transmission electron microscope operating at 200 kV (FEI Themis 60 – 300).

Electrode preparation and electrocatalytic tests

The catalyst ink was prepared by ultrasonically dispersing 5 mg of pre-catalysts into 1 mL of ethanol containing 50 μL of Nafion solution (Sigma, 5 wt %). To prepare an electrode for catalytic tests, 50 μL of pre-catalyst ink was loaded on a fine-polished GC electrode with an exposed area of 0.78 cm^2 , leading to a loading density of ca. 0.3 mg cm^{-2} (pre-catalyst + CNF supports). The electrode was then dried at room temperature (ca. 25 $^\circ\text{C}$) naturally in air. All electrocatalytic tests were carried out in a three-electrode configuration at room temperature using a Biologic VMP-3 potentiostat/galvanostat. The GC, a Pt wire and a saturated calomel electrode (SCE) were utilized as working, counter, and reference electrodes, respectively. The SCE reference was calibrated prior to each measurement in Ar/ H_2 -saturated 0.5 M H_2SO_4 solution using a clean Pt wire as the working electrode. 1.0 M KOH was used as electrolyte. Unless otherwise stated, all potentials are reported versus RHE by converting the measured potentials according to the following equation:

$$E_{\text{RHE}} = E_{\text{SCE}} + 0.059 \times \text{pH} + 0.241$$

CV was performed at a scan rate of 5 mV s^{-1} in the potential range of 1.0 to 1.8 V vs RHE. An iR -correction (85%) was made to compensate for the voltage drop between the reference and working electrodes, which was measured by a single-point high-frequency impedance measurement. Impedance spectroscopy measurements were carried out at 1.45 V vs RHE in the frequency range of 10^5 to 0.01 Hz with a 10 mV sinusoidal perturbation. The double layer capacitance of TMP pre-catalysts was estimated by performing CV in the potential range of 0.80 to 1.0 V vs RHE at different scan rates (ν) of 5, 10, 20, 30, 40, 50, 60, 70, 80, 90 and 100 mV s^{-1} , followed by extracting the slope from the resulting $|j_a - j_c|/2$ vs ν plots (j_a and j_c represent the anodic and cathodic current densities at 0.90 V vs RHE, Fig. S15 and S17f). The stability of TMP pre-catalysts was assessed using CP at a constant current density of 10 mA cm^{-2} .

Calculation of TOF

The TOF values of TMP pre-catalysts were calculated through the following equation:⁴

$$\text{TOF (s}^{-1}\text{)} = (j \times A) / (4 \times F \times n)$$

Where j (A cm^{-2}) is the current density at a given overpotential, $A = 0.78 \text{ cm}^2$ is the geometric surface area of the electrode, $F = 96500 \text{ C mol}^{-1}$ stands for the Faraday constant, n (mol) is mole number of transition metal(s) loaded on the GC electrode which was determined by the ICP-MS analysis. All metal cations in TMP were assumed to be catalytically active, so the calculated values represents the lower limits of TOF.

References

- 1 W. S. Hummers and R. E. Offeman, *J. Am. Chem. Soc.*, 1958, **80**, 1339.
- 2 J. Y. Xu, D. Aili, Q. F. Li, C. Pan, E. Christensen, J. O. Jensen, W. Zhang, G. Y. Liu, X. D. Wang and N. J. Bjerrum, *J. Mater. Chem. A*, 2013, **1**, 9737-9745.
- 3 J. Y. Li, M. Yan, X. M. Zhou, Z. Q. Huang, Z. M. Xia, C. R. Chang, Y. Y. Ma and Y. Q. Qu, *Adv. Funct. Mater.*, 2016, **26**, 6785-6796.
- 4 S. L. Zhao, Y. Wang, J. C. Dong, C. T. He, H. J. Yin, P. F. An, K. Zhao, X. F. Zhang, C. Gao, L. J. Zhang, J. W. Lv, J. Q. Liu, A. M. Khattak, N. A. Khan, Z. W. Wei, J. Zhang, S. Q. Liu, H. J. Zhao and Z. Y. Tang, *Nat. Energy*, 2016, **1**, 16184.

Supporting figures and tables

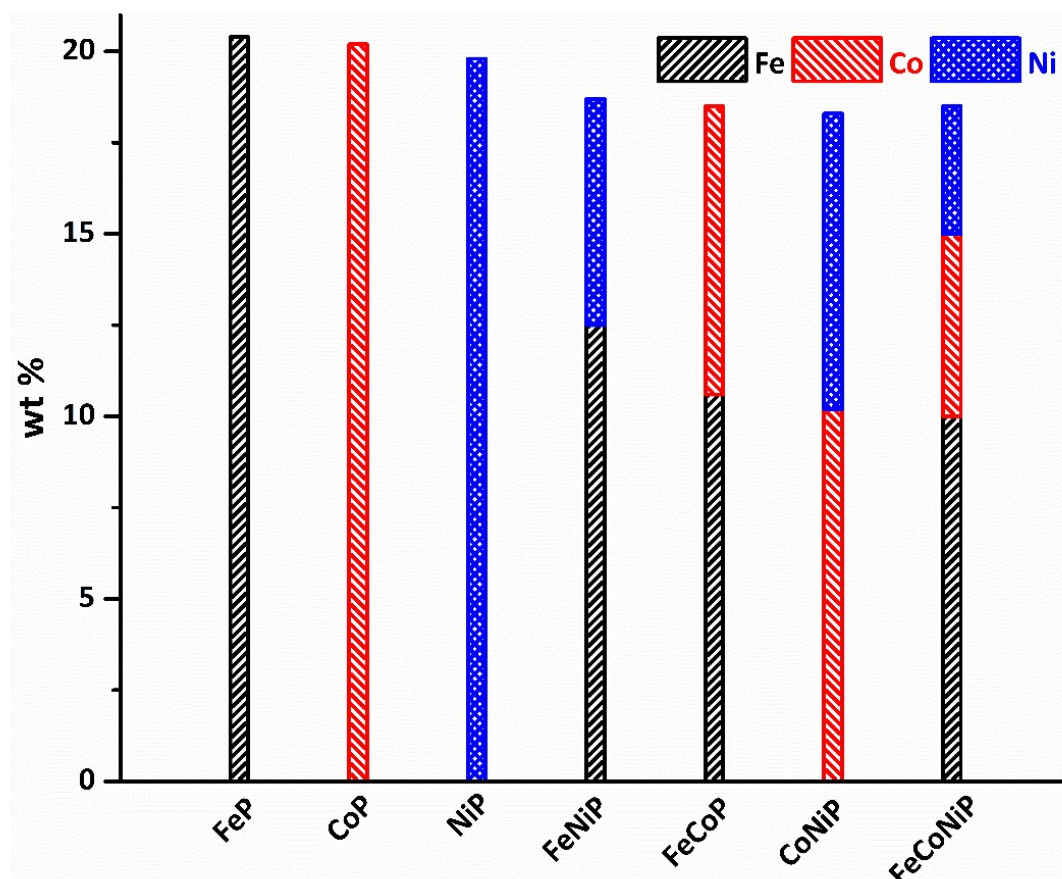


Fig. S1 The real TM content in each monophosphide pre-catalyst determined by the ICP-MS analyses.

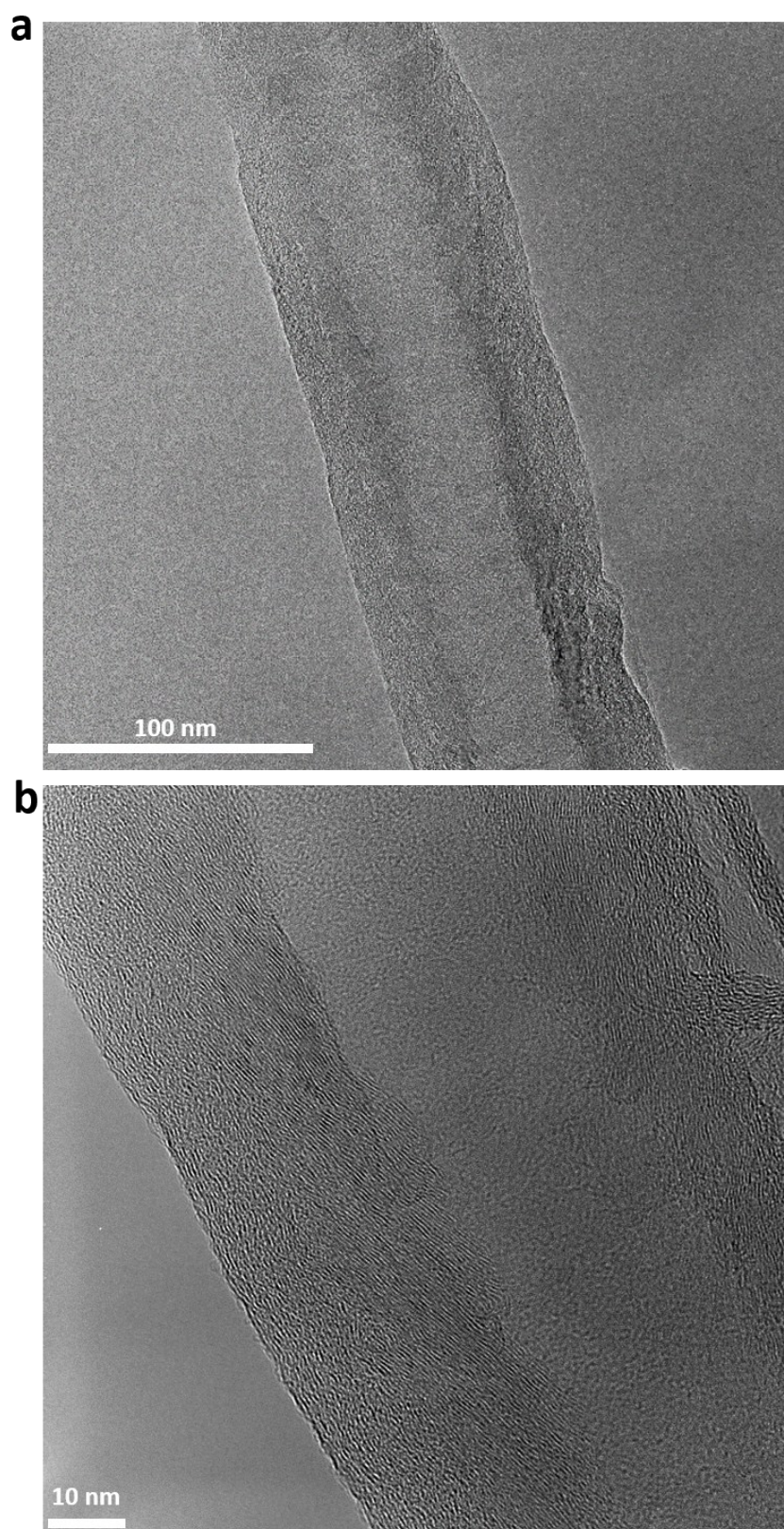


Fig. S2 TEM images of CNFs after pre-treatment in acid.

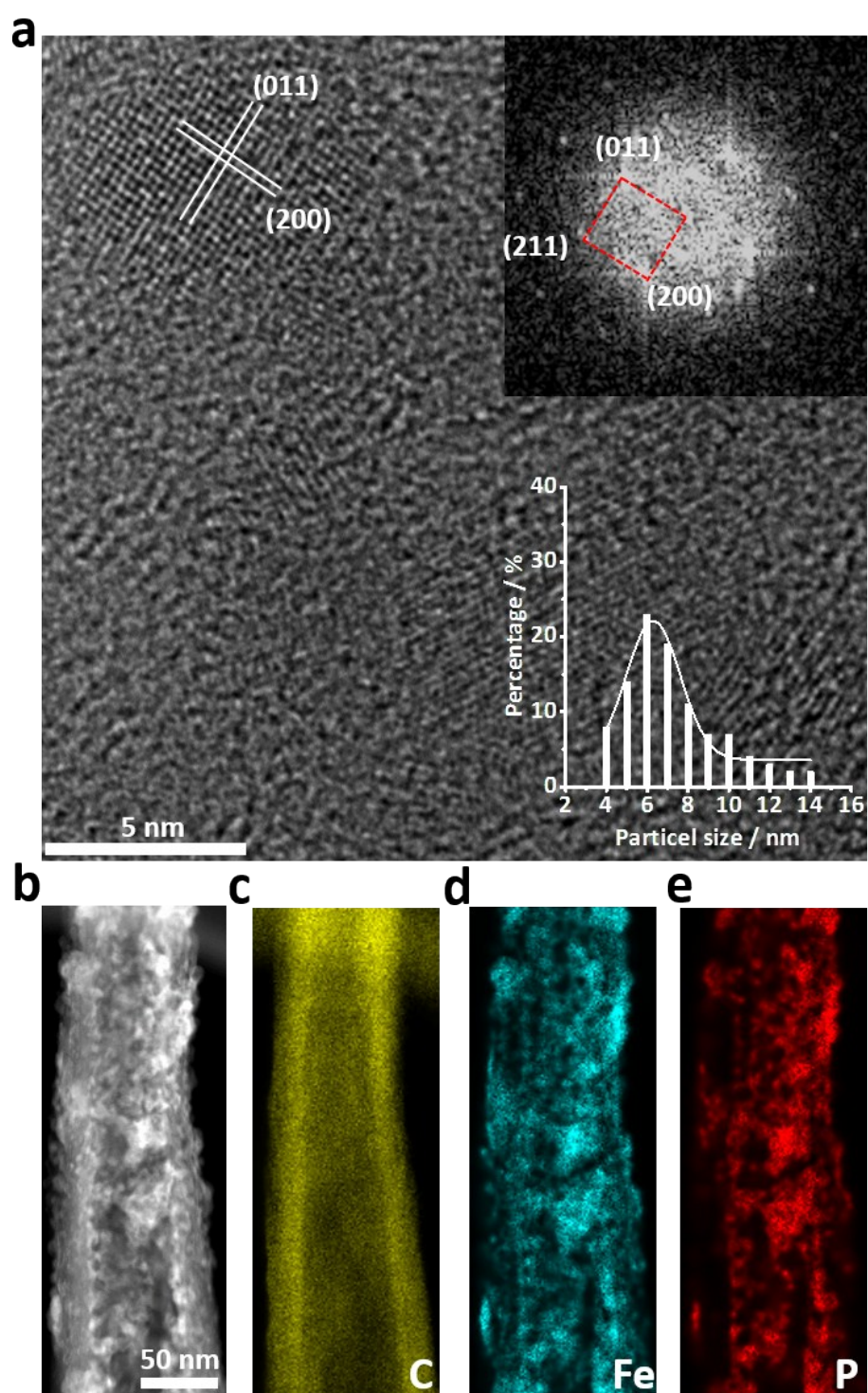


Fig. S3 TEM characterization of FeP. (a) HRTEM image of orthorhombic FeP NPs (ICDD No. 03-065-2595). Inset: particle size distribution and FFT-ED pattern. (b) STEM-HAADF image. (c-e) Elemental maps of C, Fe and P.

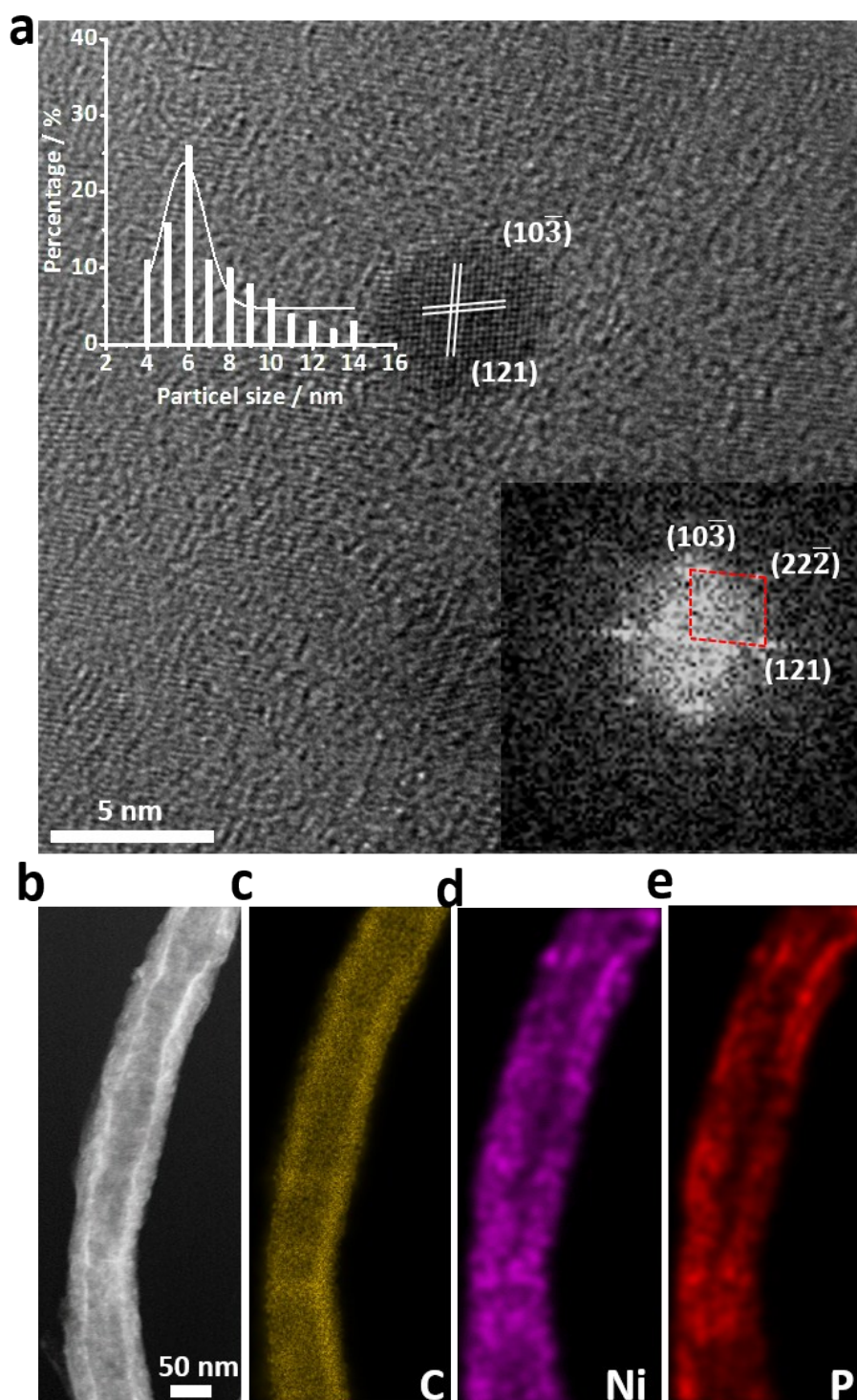


Fig. S4 TEM characterization of NiP. (a) HRTEM image of orthorhombic NiP NPs (ICDD No. 00-018-0882). Inset: particle size distribution and FFT-ED pattern. (b) STEM-HAADF image. (c-e) Elemental maps of C, Ni and P.

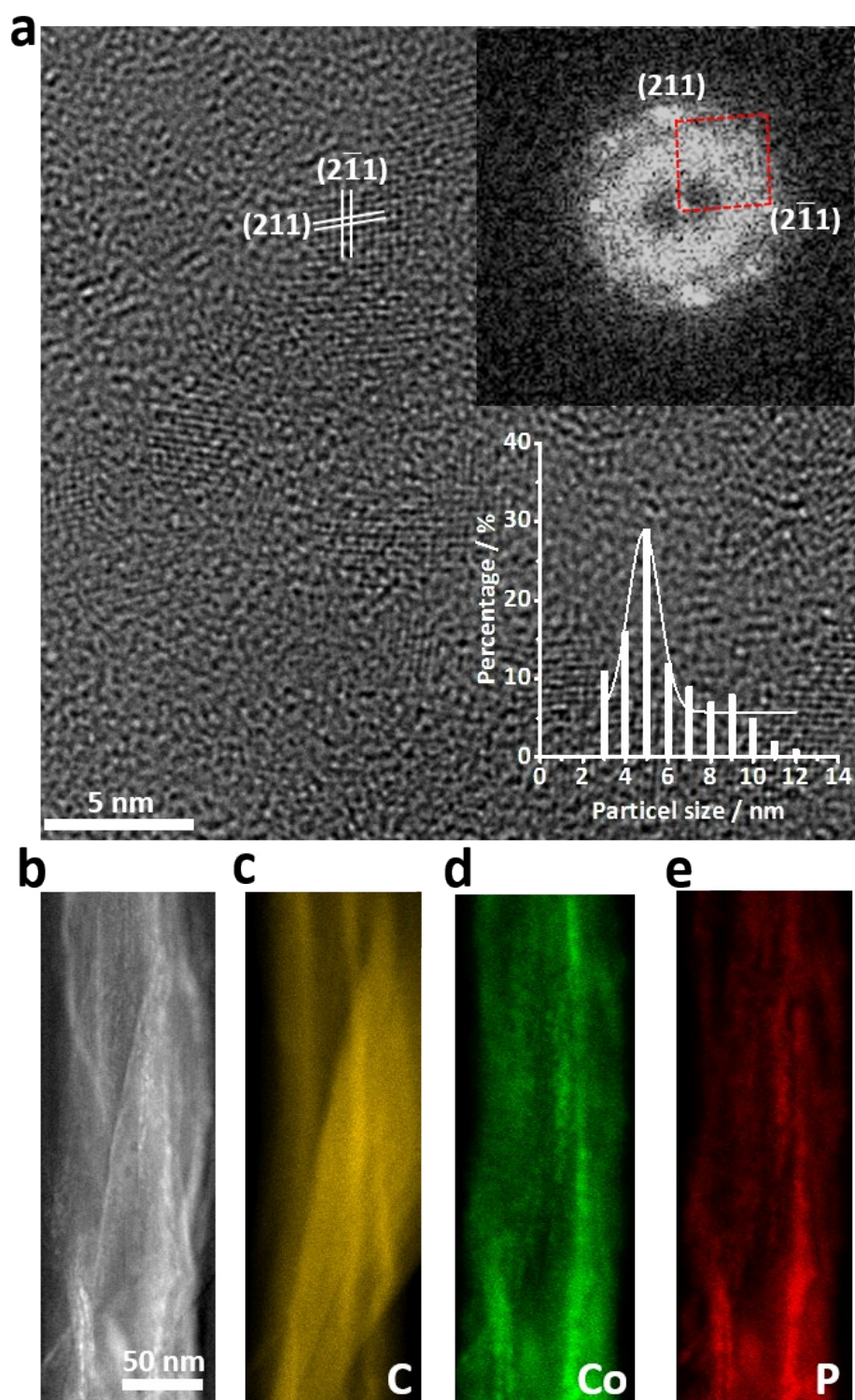


Fig. S5 TEM characterization of CoP. (a) HRTEM image of orthorhombic CoP NPs (ICDD No. 00-029-0497). Inset: particle size distribution and FFT-ED pattern. (b) STEM-HAADF image. (c-e) Elemental maps of C, Co and P.

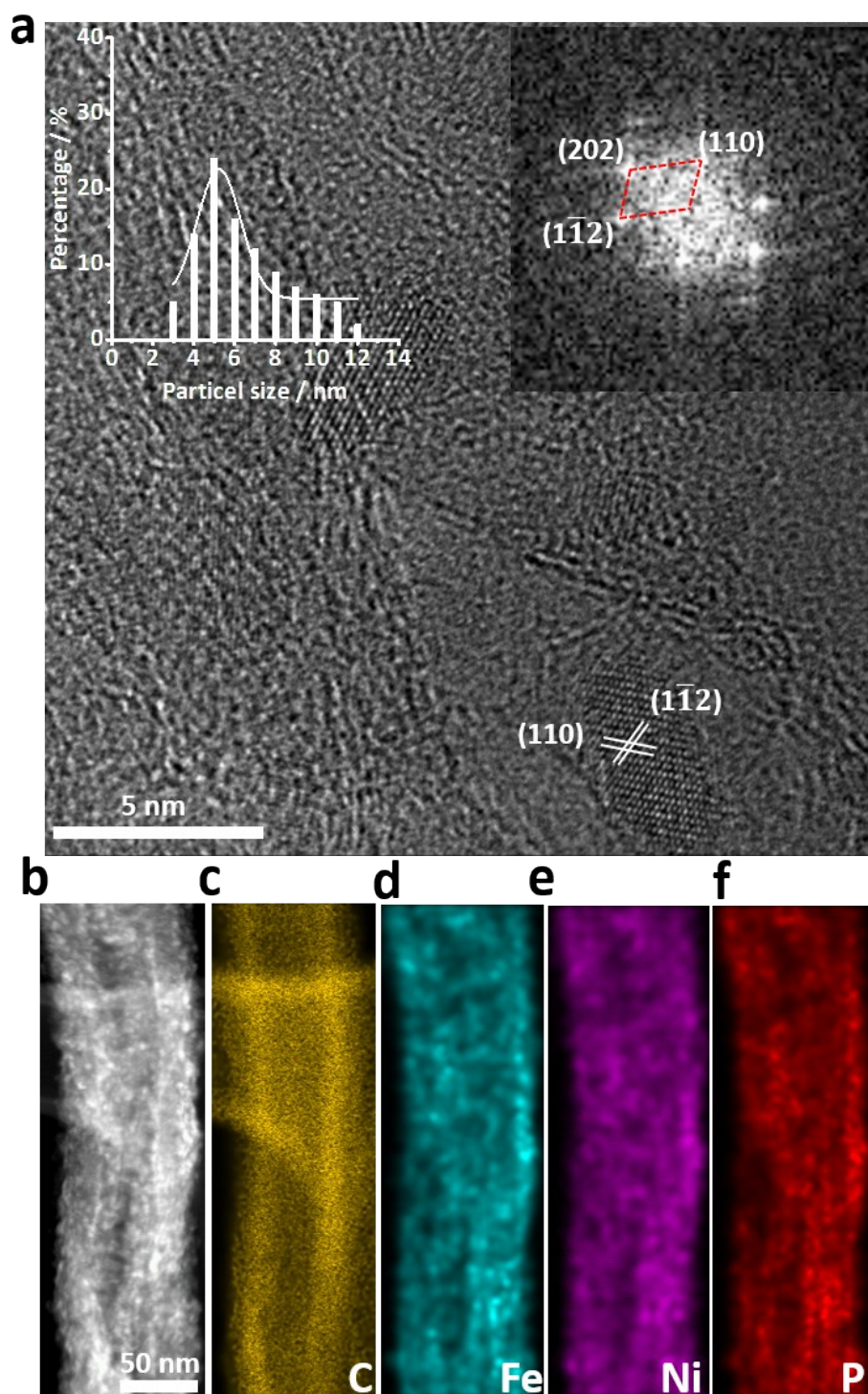


Fig. S6 TEM characterization of FeNiP. (a) HRTEM image. Inset: particle size distribution and FFT-ED pattern. (b) STEM-HAADF image. (c-f) Elemental maps of C, Fe, Ni and P.

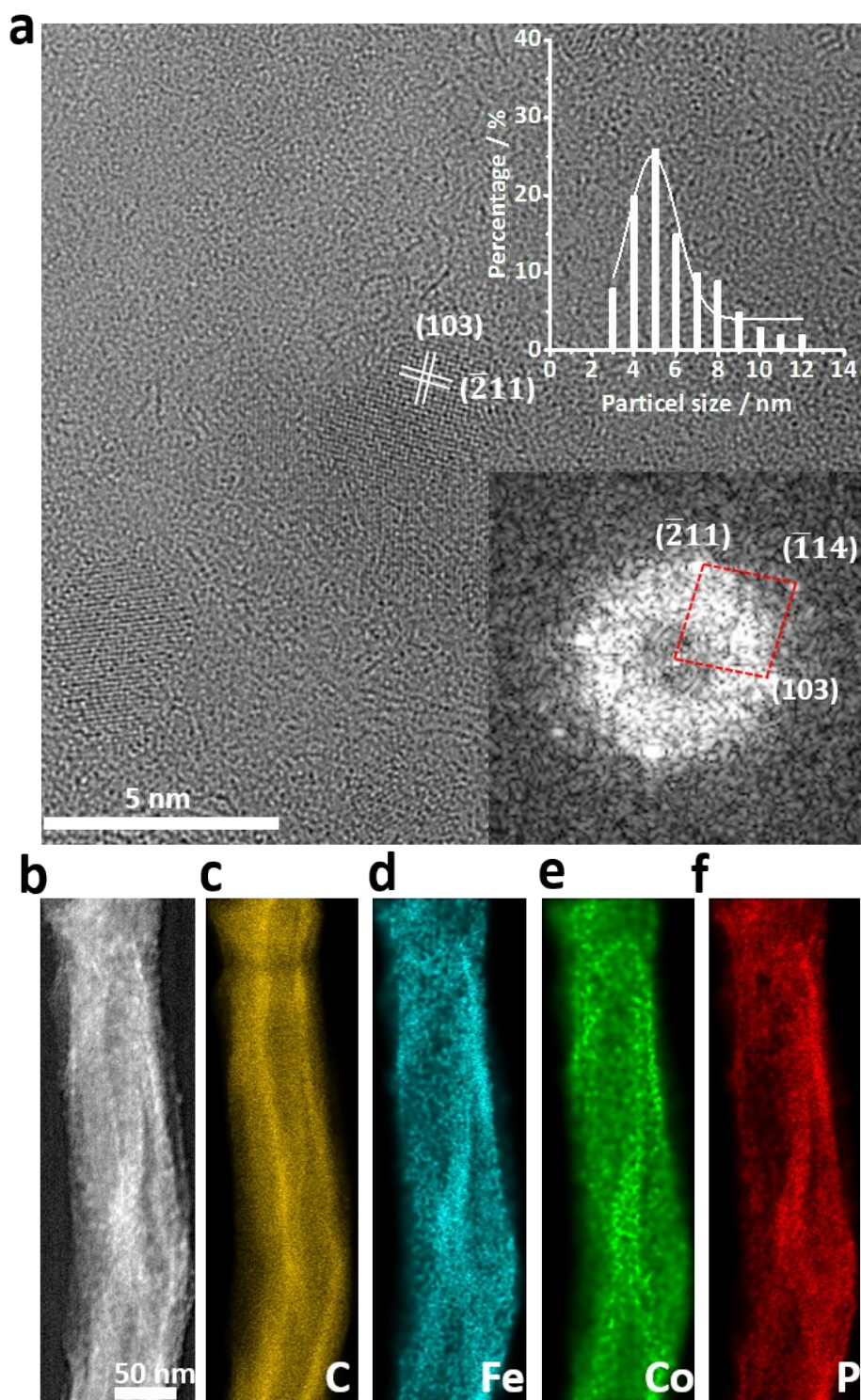


Fig. S7 TEM characterization of FeCoP. a) HRTEM image. Inset: particle size distribution and FFT-ED pattern. b) STEM-HAADF image. c-f) Elemental maps of C, Fe, Co and P.

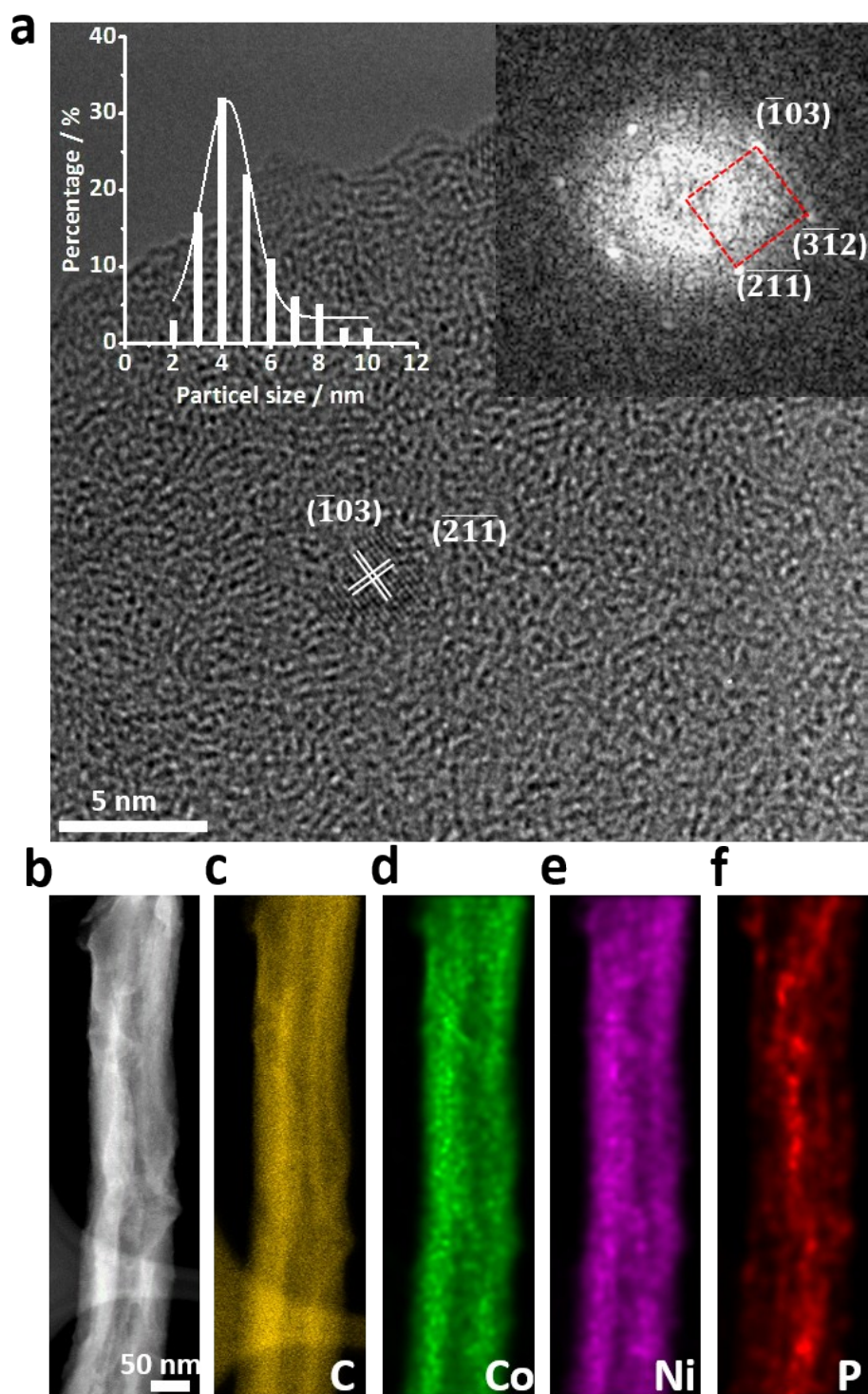


Fig. S8 TEM characterization of CoNiP. a) HRTEM image. Inset: particle size distribution and FFT-ED pattern. b) STEM-HAADF image. c-f) Elemental maps of C, Co, Ni and P.

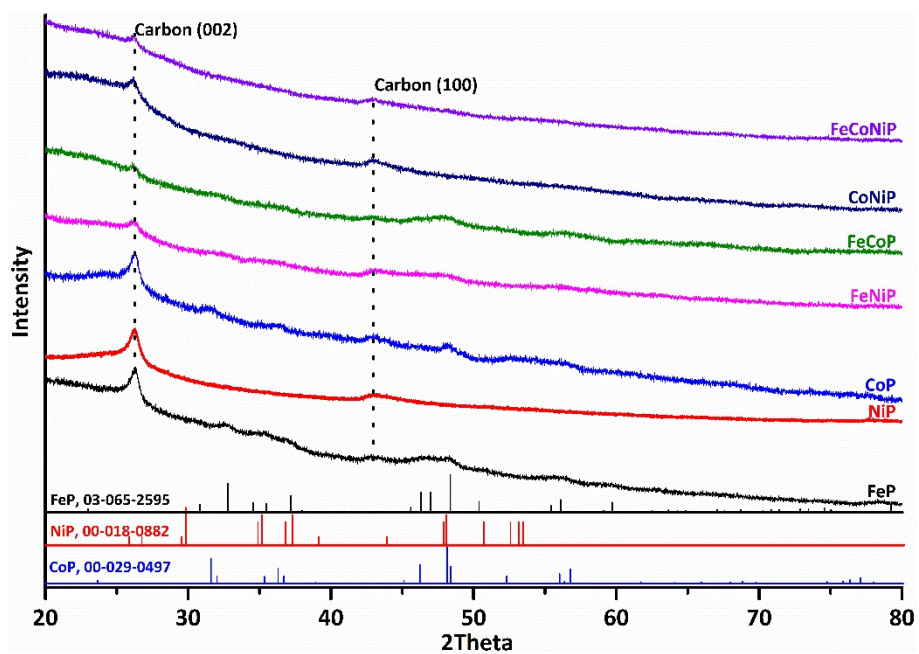


Fig. S9 XRD patterns of TMP pre-catalysts. The standard powder diffraction patterns of orthorhombic FeP (ICDD No. 03-065-2595), orthorhombic NiP (ICDD No. 00-018-0882) and orthorhombic CoP (ICDD No. 00-029-0497) are given for reference.

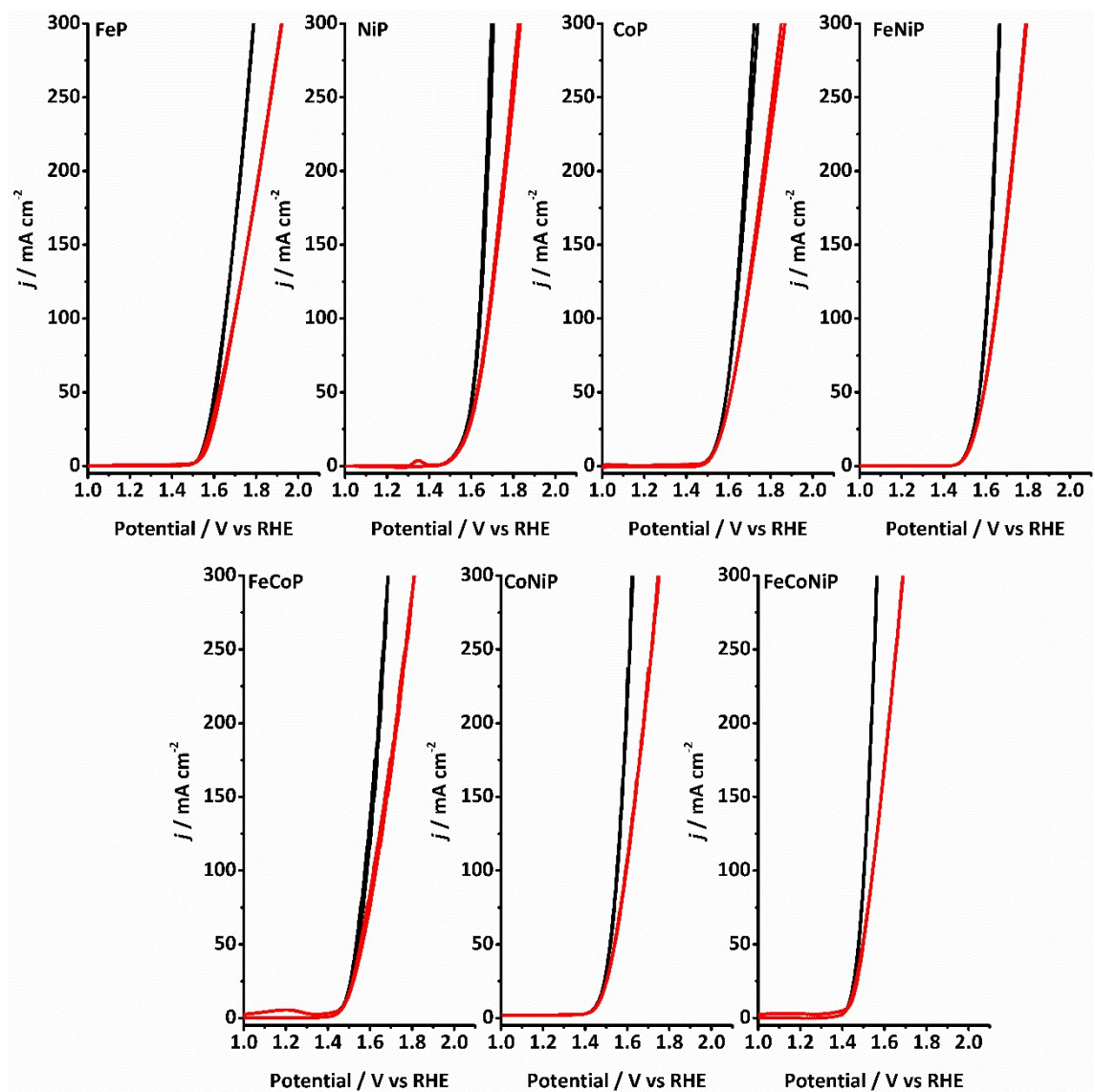


Fig. S10 The CV curves of TMP pre-catalysts after pre-activation with (black) and without (red) iR -correction.

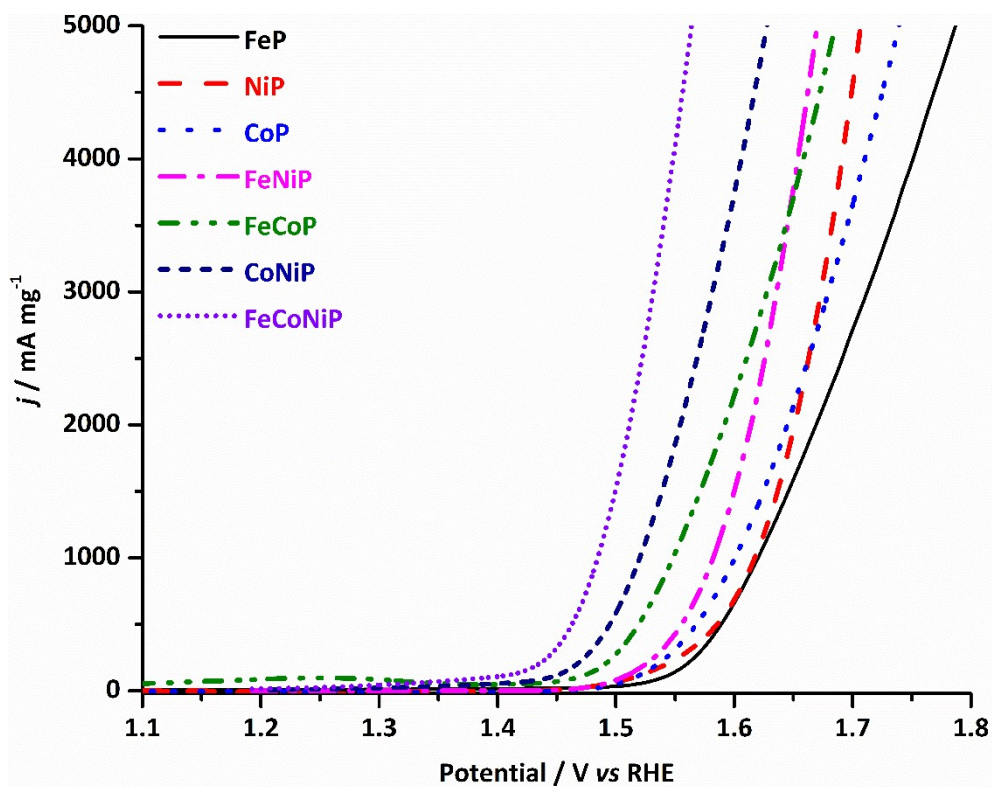


Fig. S11 OER mass activity of the TMP pre-catalysts normalized based on the total loadings of transition metals.

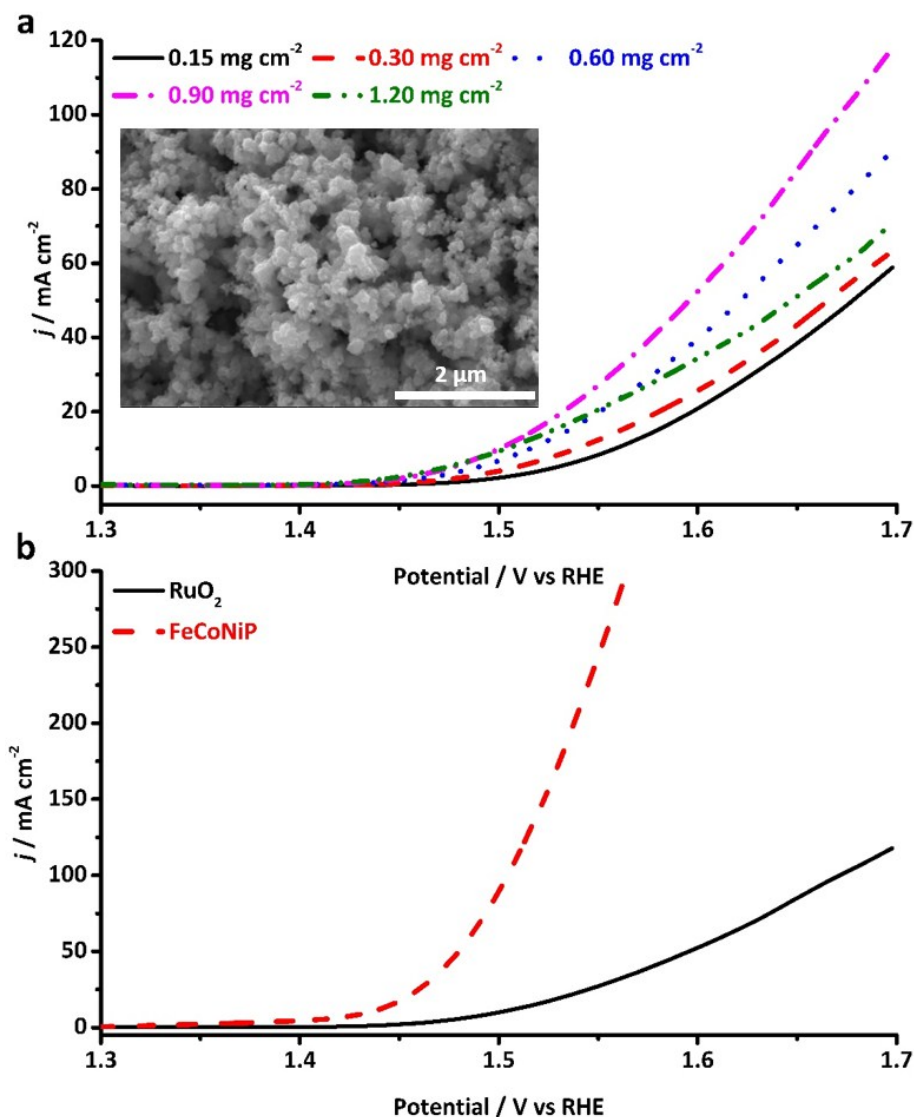


Fig. S12 (a) Polarization curves showing the OER performance of commercial RuO_2 NPs with different loadings. Inset: representative SEM image of RuO_2 NPs. b) Polarization curves showing the comparison of OER activity between FeCoNiP and RuO_2 . The measurements were conducted in 1.0 M O_2 -saturated KOH electrolyte at room temperature.

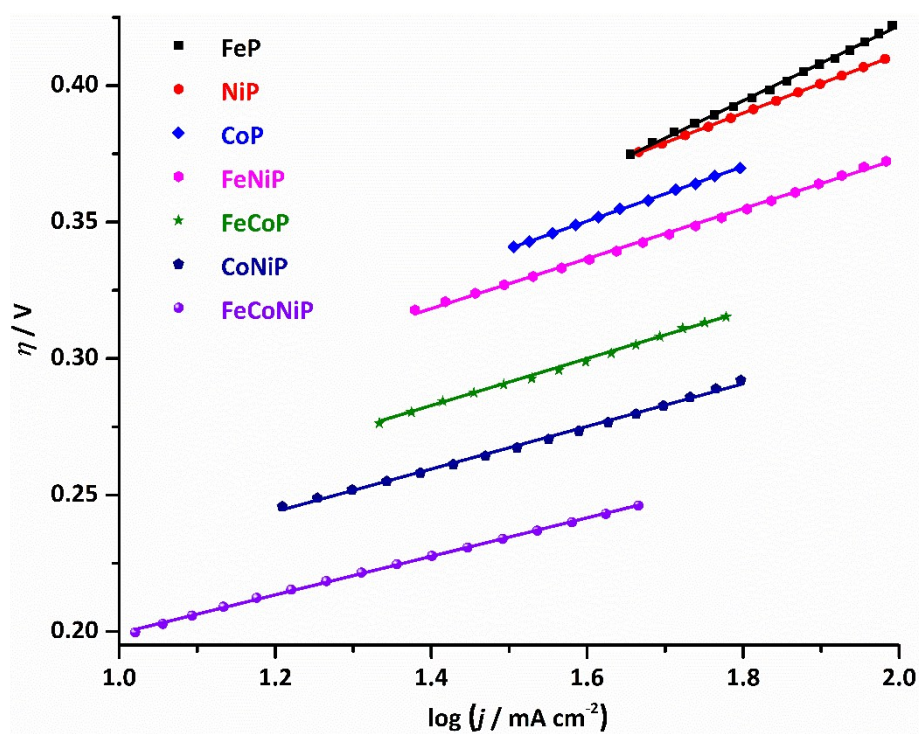


Fig. S13 Tafel plots of the TMP pre-catalysts in the overpotential range of 0.2 – 0.42 V.

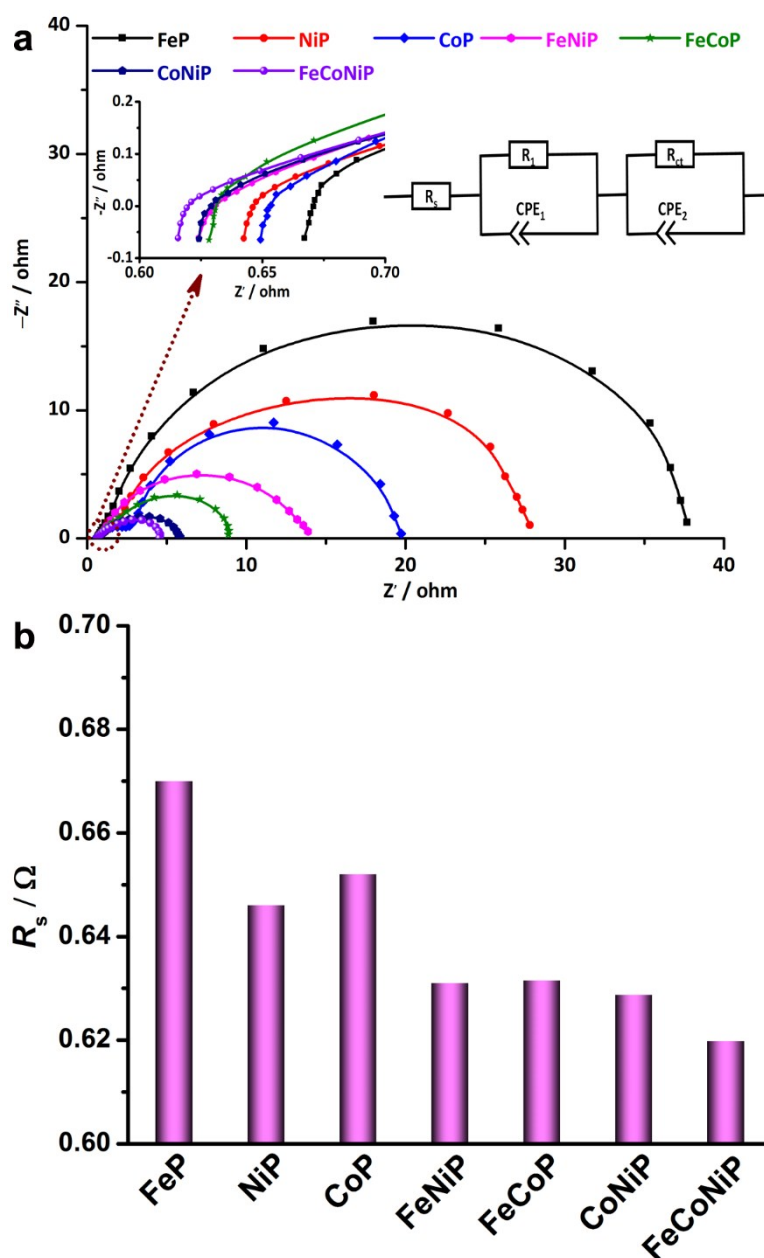


Fig. S14 (a) The Nyquist plots of the TMP pre-catalysts measured at 1.45 V vs RHE. Scattered dots are experimental data points and solid lines are fitting curves. The insets show the zoomed view of the plots in the high frequency regions (left) and the equivalent circuit model used for fitting (right). R_s and R_{ct} represent the equivalent series resistance and charge transfer resistance, respectively. CPE stands for the constant phase element. (b) Comparison of R_s values of all TMP pre-catalysts, which to a certain extent reflect the ohmic resistance of the catalytic materials (resistance from glassy carbon, lead and electrolyte was fixed in our experiments).

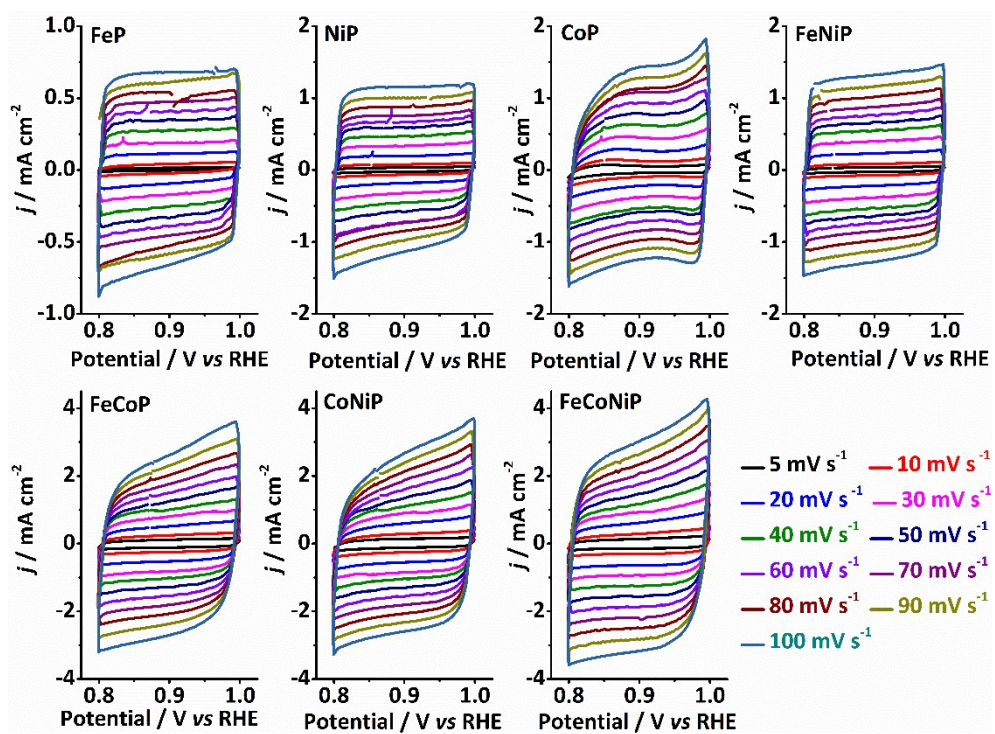


Fig. S15 Electrochemical CV curves of TMP pre-catalysts recorded at different scan rates of 5, 10, 20, 30, 40, 50, 60, 70, 80, 90 and 100 mV s⁻¹.

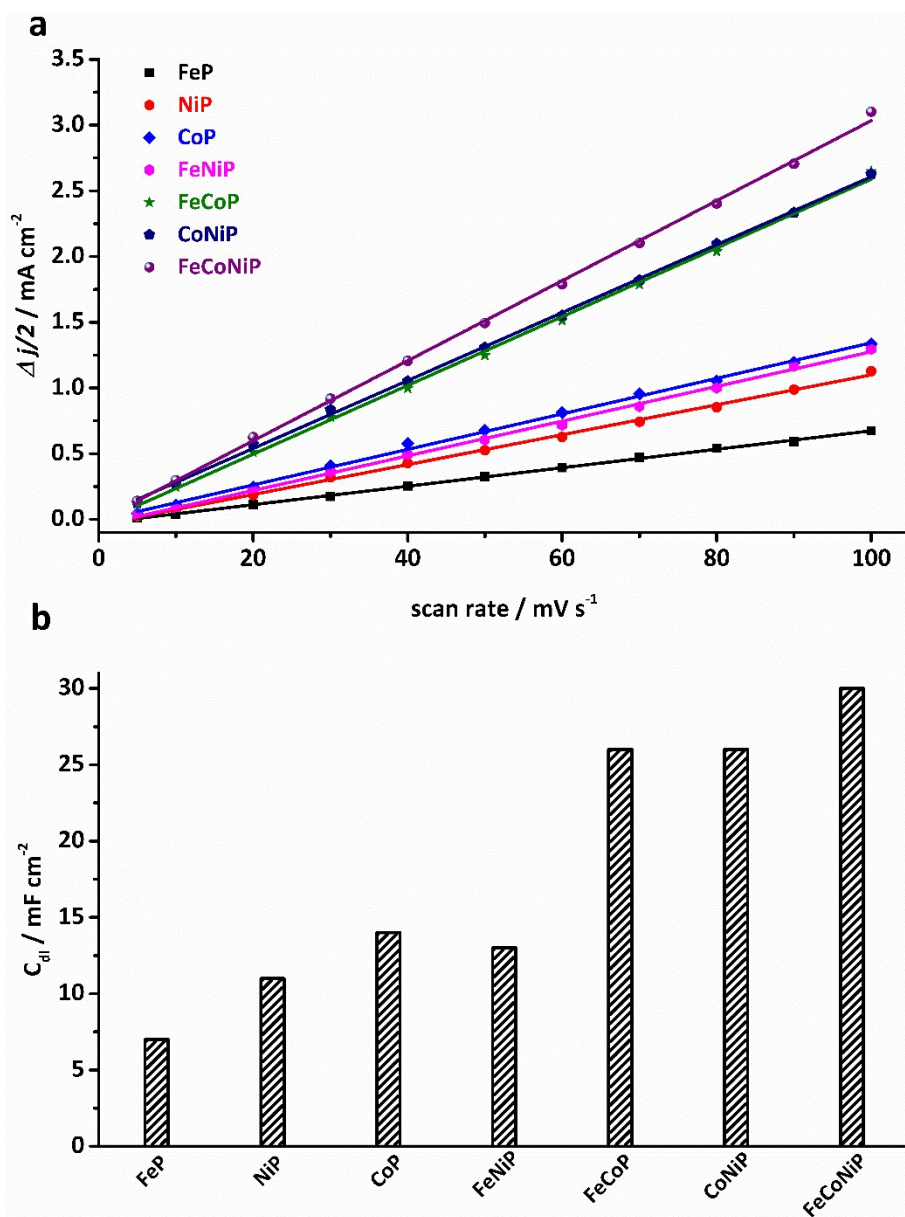


Fig. S16 (a) Plots of the capacitive currents as a function of the scan rate for each TMP pre-catalyst. (b) C_{dl} value for each TMP pre-catalyst.

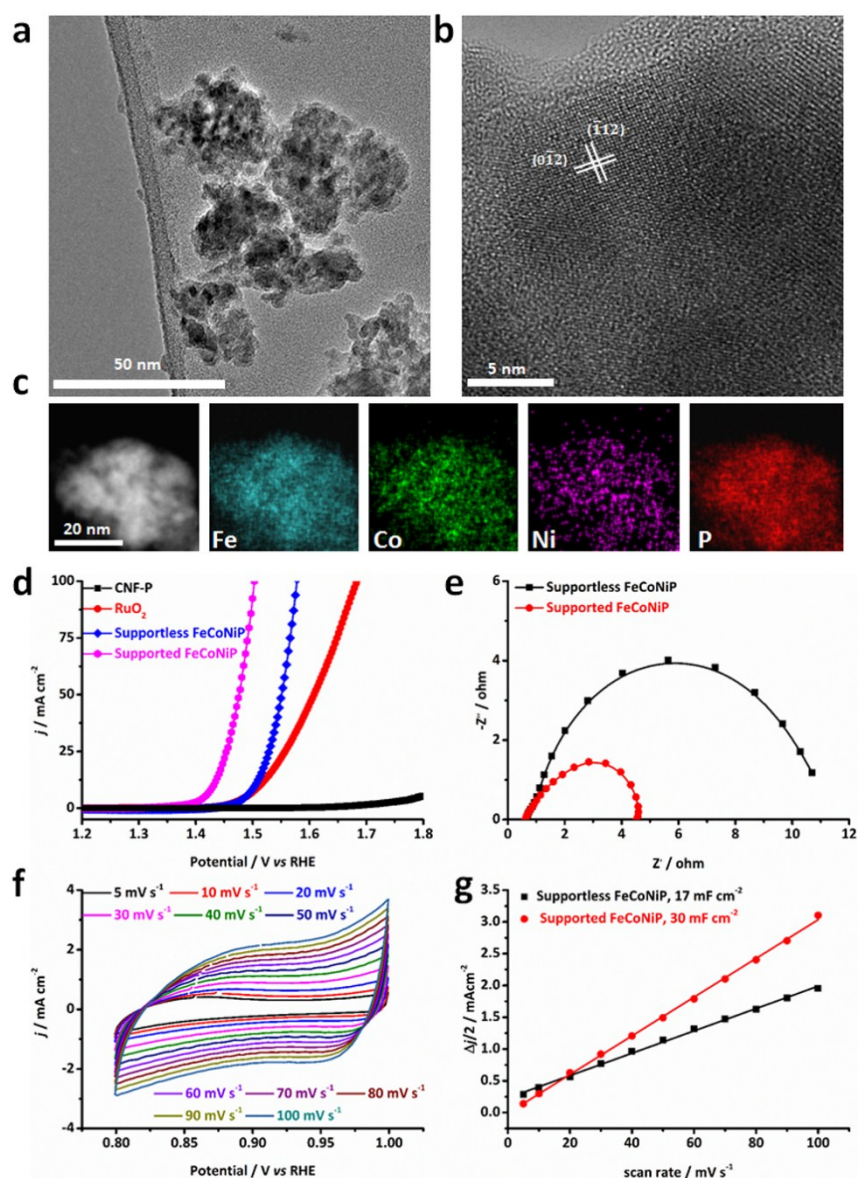


Fig. S17 Microstructural and electrochemical characterization of supportless FeCoNiP pre-catalysts. (a) TEM image. (b) HRTEM image showing the same orthorhombic structure as that observed in CNF-supported FeCoNiP. (c) HAADF-STEM image and elemental maps of Fe, Co, Ni and P of supportless FeCoNiP. (d) iR -corrected polarization curves of the CNF-P support, RuO_2 control catalyst (the best-performing one shown in **Fig. S12**), supportless FeCoNiP and supported FeCoNiP, recorded at a scan rate of 5 mV s^{-1} in the potential range of 1.0 to 1.8 V vs RHE. (e) The Nyquist plots of supportless and supported FeCoNiP pre-catalysts measured at 1.45 V vs RHE. (f) CV plots showing the capacitive current as a function of the scan rate for supportless FeCoNiP. (g) C_{dl} values of the supportless and supported FeCoNiP pre-catalysts.

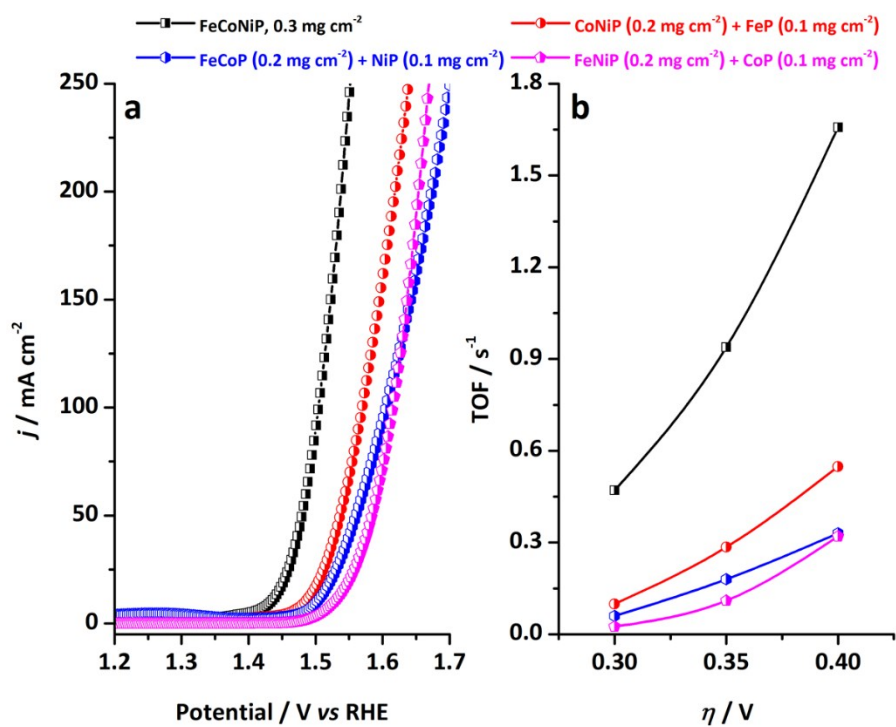


Fig. S18 Comparison of the OER activity of FeCoNiP pre-catalysts with physically mixed mono- and bi-metallic TMP pre-catalysts (i.e. CoNiP + FeP, FeCoP + NiP, and FeNiP + CoP). The total metal loadings of all pre-catalysts were kept the same. (a) The apparent OER activities. (b) TOF values calculated at $\eta = 300, 350$ and 400 mV .

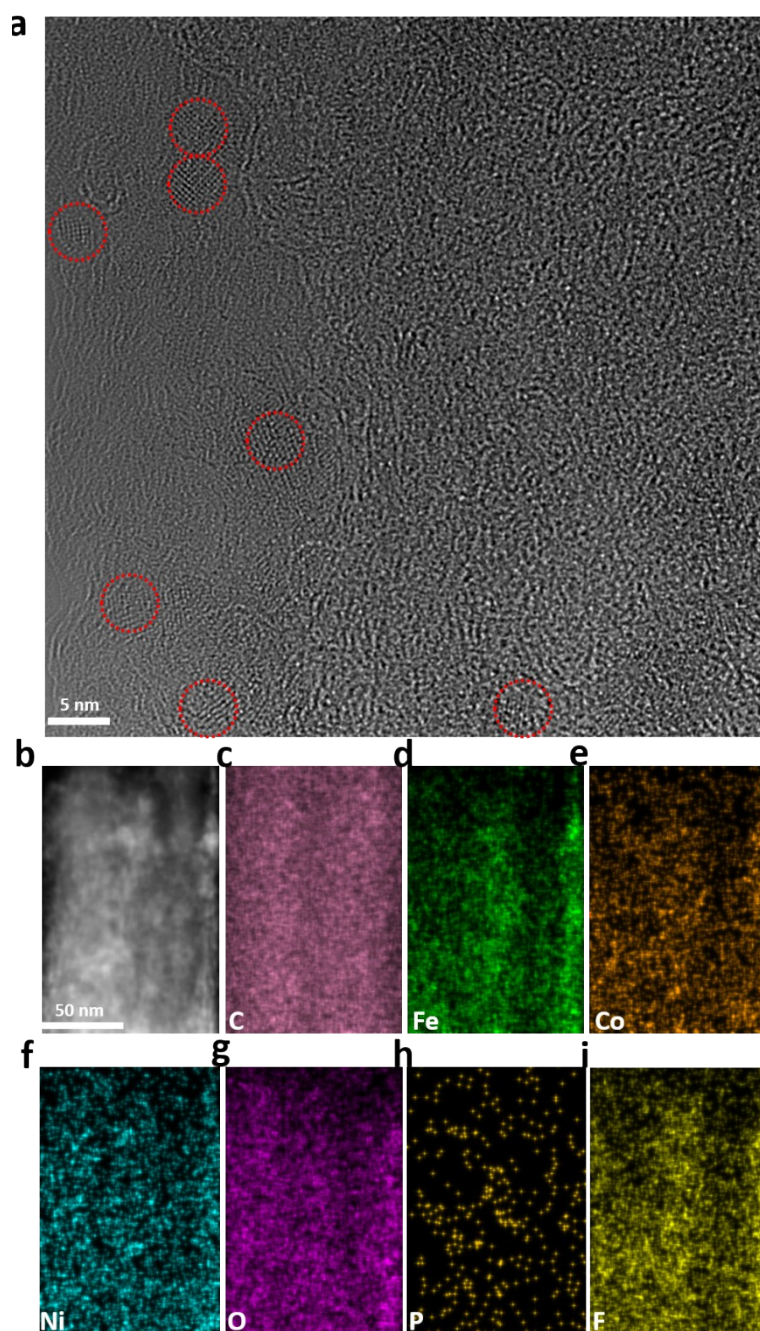


Fig. S19 TEM characterization of the FeCoNiP pre-catalysts after activation. (a) HRTEM image, (b) STEM-HAADF image, (c-i) Elemental maps of C, Fe, Co, Ni, O, P and F.

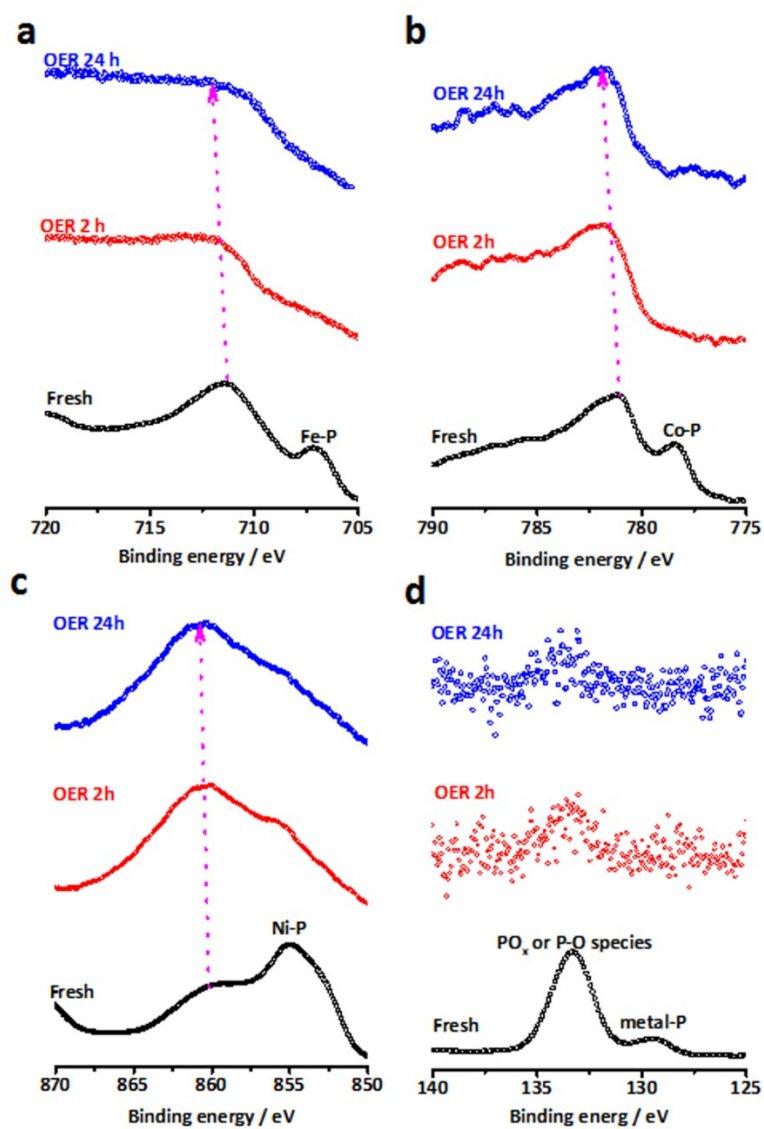


Fig. S20 XPS spectra of the as-prepared FeCoNiP pre-catalysts and the FeCoNiP pre-catalysts subjected to OER electrolysis at a constant current density of 10 mA cm⁻² for 2 and 24 h. (a) Fe 2p_{3/2}, (b) Co 2p_{3/2}, (c) Ni 2p_{3/2} and (d) P 2p.

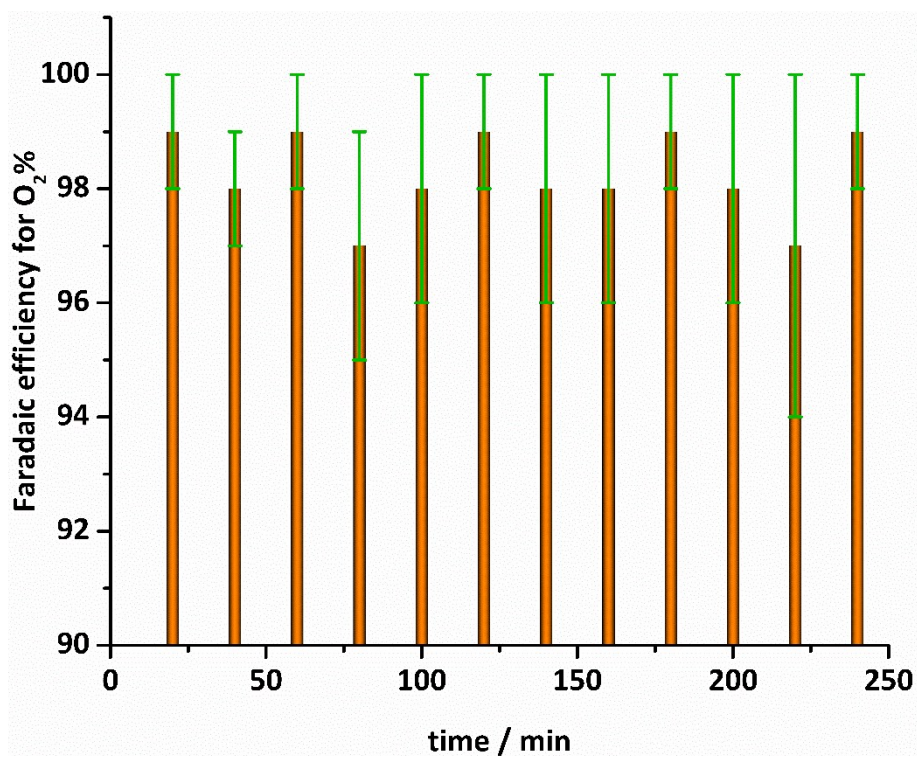


Fig. S21 Faradaic efficiency of the FeCoNiP pre-catalysts for oxygen evolution measured at 50 mA cm⁻².

Table S1. Comparison of OER performance with the various of state-of-the-art catalysts in 1.0 M KOH electrolyte.

Catalysts	Substrate	Loading (mg cm ⁻²)	η_j / mV			TOF η / s ⁻¹		References
			η_{10}	η_{50}	η_{100}	TOF ₃₀₀	TOF ₃₅₀	
FeCoNiP nanoparticle	Glassy carbon	TM ca. 0.06	200	248	270	0.47	0.94	This work
Fe ₁₀ Co ₄₀ Ni ₄₀ P nanosheet array	Ni foam	3.1	250	277	295	ca. 0.007	/	RSC Adv., 2016, 6, 9647.
Ni _{1.5} Fe _{0.5} P/CF nanosheet	Carbon paper	1.38	264	ca. 279	293	ca. 0.014	/	Nano Energy, 2017, 34, 472.
Co _{0.7} Fe _{0.3} P/CNT nanoparticle	Carbon paper	0.5	243	ca. 270	/	/	/	Adv. Funct. Mater., 2017, 27, 1606635.
CoNiP ultrathin nanosheet	Glassy carbon	0.153	273	ca. 330	ca. 365	ca. 0.028	ca. 0.09	Energy Environ. Sci., 2017, 10, 893.
	Ni foam		209	ca. 257	ca. 275	ca. 0.32	/	
Fe _{1.1} Mn _{0.9} P Nanorod	Glassy carbon	0.284	440	/	/	/	/	Chem. Mater., 2017, 29, 3048.
Al-CoP/CC nanoarray	Carbon cloth	5.7	265	ca. 300	ca. 340	ca. 0.0015	ca. 0.0017	Nanoscale, 2017, 9, 4793.
FeCoP nanoarray	Ti foil	1.03	230	ca. 290	310	ca. 0.013	ca. 0.022	Adv. Mater., 2017, 29, 1602441.
O-CoP/GO nanoparticle	Glassy carbon	0.28	280	/	440	0.01	0.018	J. Am. Chem. Soc., 2016, 138, 14686.
Nanoporous (Co _{0.52} Fe _{0.48}) ₂ P	CoFe ribbon	/	270	ca. 290	/	/	/	Energy Environ. Sci., 2016, 9, 2257.
NiCoP/GO nanoparticle	Carbon paper	Phosphide 0.15	270	ca. 360	ca. 430	ca. 0.047	ca. 0.062	Adv. Funct. Mater., 2016, 26, 6785.
Ni _{0.51} Co _{0.49} P film	Ni foam	/	239	ca. 270	ca. 320	/	/	Adv. Funct. Mater., 2016, 26, 7644.
NiCoP nanosheet array	Ni foam	/	/	308	ca. 340	/	/	Nano Res., 2016, 9, 2251.
CoMnP nanoparticle	Glassy carbon	0.284	330	/	/	ca. 0.004	/	J. Am. Chem. Soc., 2016, 138, 4006.
NiCoP nanoplate (Co _{0.54} Fe _{0.46}) ₂ P nanoparticle	Ni foam	1.6	280	ca. 350	/	3.88 ^a	/	Nano Lett., 2016, 16, 7718.
	Glassy carbon	0.2	370	/	/	/	/	Angew. Chem. Int. Ed., 2015, 54, 9642.
Ni _{0.69} Co _{0.31} P yolk-shell sphere	Carbon paper	3.5	266	ca. 315	350	0.15 ^a	0.68 ^a	Nanoscale, 2016, 8, 19129.
FeP nanorod	Carbon paper	0.7	350	ca. 450	ca. 530	ca. 0.0016	ca. 0.0032	Chem. Commun., 2016, 52, 8711.
FeP nanotube	Carbon cloth	/	288	ca. 320	ca. 360	/	/	Chem. Eur. J., 2015, 21, 18062.
CoP film	Cu foil	/	345	ca. 380	413	/	/	Angew. Chem. Int. Ed., 2015, 54, 6251.
CoP mesoporous nanorod array	Ni foam	/	290	ca. 330	ca. 370	/	/	Adv. Funct. Mater., 2015, 25, 7337.
Porous urchin-Like Ni ₂ P	Ni foam	/	200	ca. 240	268	/	0.015	ACS Catal., 2016, 6, 714.
Ni ₅ P ₄ film	Ni foil	/	320	ca. 370	/	/	/	Angew. Chem. Int. Ed., 2015, 54, 12361.
N ₂ P nanowire	Glassy carbon	0.14	290	/	/	ca. 0.021	/	Energy Environ. Sci., 2015, 8, 2347.
Nitrogen-doped carbon nanoparticle	Rotating ring-disk electrode	0.2	380	ca. 580	/	/	/	Nat. Commun., 2013, 4, 2390.
3D porous nitrogen-doped carbon	Carbon cloth	/	410	ca. 560	/	/	/	Energy Environ. Sci., 2016, 9, 1210.
NiFeO _x /CFP nanoparticle	Carbon paper	1.6	230	ca. 260	ca. 300	ca. 0.012	/	Nat. Commun., 2015, 6, 7261.
Porous MoO ₂ nanosheet	Ni foam	2.9	260	/	/	/	/	Adv. Mater. 2016, 28, 3785.
Co _{0.8} Se/NiFe-LDH nanosheet	Glassy carbon	4	/	/	270	ca. 0.016	/	Energy Environ. Sci., 2016, 9, 478.
Ni _{0.75} V _{0.25} -LDH nanosheet	Glassy carbon	0.143	300	ca. 390	/	ca. 0.0216	0.054	Nat. Commun. 2016, 7, 11981.
Nanoporous G-FeCoW	Glassy carbon	0.20	223	ca. 280	/	0.46	/	Science, 2016, 352, 333.
	Au foam		191	ca. 230	ca. 280	/	/	
Ni ₃ S ₂ nanosheet array	Ni foam	1.6	260	/	/	ca. 0.003	/	J. Am. Chem. Soc., 2015, 137, 14023.
NiCo ₂ S ₄ nanowire array	Ni foam	/	260	ca. 350	ca. 390	/	/	Adv. Funct. Mater., 2016, 26, 4661.
CoSe ₂ sheet	Glassy carbon	/	270	ca. 440	/	/	/	Angew. Chem. Int. Ed. 2015, 54, 12004.
Ni ₃ Se ₂ film	Ni foam	0.22	290	ca. 470	ca. 670	0.044	ca. 0.052	Energy Environ. Sci., 2016, 9, 1771.
NiCo-UMOFNs nanosheet	Glassy carbon	0.20	250	ca. 290	/	0.18	/	Nat. Energy, 2016, 1, 16184.
	Cu foam	/	189	ca. 260	/	0.86	/	

^a The TOF was calculated based on the surface active site, not all the loaded catalysts.

^b The ca. η_j was concluded from the performance curves in the literature.

^c The ca. TOF_j was concluded from the current densities and all the loadings listed in the literature.